Proposal for an All-Optical Intra-Pulse Instantaneous Frequency Measurement

André Paim Gonçalves, Felipe Araújo Marins, Danilo M. Olivieri [1], Ricardo Marques Ribeiro[2], Felipe Streitenberger Ivo, Olympio Lucchini Coutinho[3]

[1] Instituto de Pesquisa da Marinha (IPqM), Rio de Janeiro/RJ - Brasil

[2] Universidade Federal Fluminense (UFF), Niterói/RJ – Brasil

[3] Instituto Tecnológico de Aeronáutica (ITA), São José dos Campos/SP – Brasil

***Abstract* – This article presents a new concept of Instantaneous Frequency Measurement (IFM) performed at the receiver, which is based on Microwave Photonics. The implementation of IFM has the capability of measuring RF intra-pulse parameters. The proposed optical circuit is based on the concept of optical self-homodyning, where the carrier and one of the sidebands are eliminated. The remaining sideband is inserted into an MZI with arms of different sizes coupled to a low-speed photodetector. This process produces a tone increased by the spectral components of the measured RF signal envelope because of the spectral components of the remaining sideband beating in the photodetector. The proposed optical circuit brings the benefit of employing simpler digitizers, reducing system latency, and has the possibility of being transformed into a photonic integrated circuit (PIC). It was predicted by mathematical deduction, and the concept was experimentally confirmed.**

***Index Terms* – Instantaneous Frequency Measurement (IFM), Instantaneous Wideband, Microwave Photonics.**

I. INTRODUCTION

Microwave Photonics (MWP) is an area of human knowledge that since the 1970's has been consolidated as the study of photonic devices operating in microwave frequencies and their application in microwave systems. The initial idea was to use the advantages of photonic technologies to provide functions in overly complex microwave systems instead of directly making an approach that is difficult or impossible in the field of radio frequency (RF). These advantages come with low weight, volume and power consumption, as well as their band [1]. Using the knowledge developed by MWP, the development of the photonics intra-pulse parameter IFM receiver was sought to become a new choice related to those implemented by electronics.

The mainly electronic warfare devices use conventional IFM receiver, presenting better performance than other devices in terms of wideband operation range, high probability of intercept, large dynamic range and high measurement accuracy. This electronic device can measure frequency for pulsed and continuous-wave (CW) microwave signals, also it can estimate other significant pulse parameters including pulse width (PW), pulse amplitude (PA), interval of repetition of the pulse (IRP) and time of arrival (TOA) within a wide frequency range [2]. However, conventional IFM receivers have limited instantaneous bandwidth, large frequency-dependent loss and susceptibility to electromagnetic interference (EMI) [3].

A. P. Gonçalves, andrepg43@yahoo.com.br; F. A. Marins, amarins.felipe@gmail.com; R. M. Ribeiro, rmr@telecom.uff.br; D. M. Olivieri, danilo.olivieri@marinha.mil.br; F. S. Ivo, fivo@ita.br; O. L. Coutinho, olympio@ita.br.

.

The digital IFM electronic receivers have become, in the last years, a great promise. They are implemented by digital signal processing (DSP). These devices use the integrated circuit called the field-programmable gate array (FPGA). The process begins when the RF signal received is amplified by the low noise amplifier (LNA) and then passes throw to the mixer to suffer heterodyne process. The result is a signal down-converted to an intermediate frequency (IF) [2]. The analog to digital converters (ADC) of the FPGA digitalizes the IF signal. This process allows a flexible approach to implement RF signal processing. However, the electronic IFM technique brings a lot of complication with RF down-converting, digitalization and latency. The RF down-conversion process can introduce spurious frequencies. The digitalization process brings a quantization noise. The quantization noise is a critical problem to handle in a FPGA project since this is an unavoidable consequence of signal digitization. The increasing range of voltage level diversity is desirable to obtain more precision. Nonlinear characteristics of the digitalization process can produce unwanted natural harmonics. The latency of the system can be a limitation for many applications like ESM (Electronic Support Measurement) for example. In hard electromagnetic environment, when there are so many RF signals to process at same time, there is a physical limitation for CMOS system. Almost all of this signal processing systems is constrained by CMOS technology [4]. Another kind of digital IFM was proposed without frequency down-conversion thus avoiding the problem of spurious frequency introducing called Direct RF Sampling [5]. There are two kinds of Direct RF sampling. The first kind uses a single fixed clock and for low RF frequencies it works well, but for high RF frequencies it has problems related to the effect of clock jitter or clock uncertainty [6]. The second kind uses the tunable RF sample clock. This process has a problem when the RF sample clock modulation induces a Nyquist-zone dependent frequency modulation on the received signals [7]. The direct RF sampling detection process depends on one technique called pulse sampling. This is a technique that can be used for much higher frequencies than track and hold-based sampling. The basics requirements for high RF pulse sampling are narrow pulse width and low pulse amplitude jitter. In addition to the low time jitter is also required in any direct RF sampling scheme [5]. These devices use ADC to make down-conversion directly, but it brings RF operation band limitations, today, the electro-optical modulators have input frequency band greater than ADC [8]. The power consumption is another limitation of the ADC relation to optical devices [9].

In recent years, the MPW has become attractive for IFM development because of its high bandwidth and low latency

[8], [9] and [10]. The excellent review the field of microwave photonics instantaneous frequency measurements (IFM) was reported and all of the structure analyzed by [11] and [12]. During bibliographic research it was not possible to find works that refer to the method proposed in this article. A photonic approach here is proposed to measure multiple intra-pulse parameters of complex microwave signals for the first time.

Reference [3] describes an approach where the intra-pulse parameters (i.e., carrier frequency, PA, PW, PRF, symbol rate and modulation format) can be identified through the analysis of the instantaneous amplitudes detected at the two outputs of the dual-port Mach–Zehnder interferometer (MZI), instantaneous Amplitude Comparison Function (ACF), and instantaneous frequency. The proposed approach can measure complex microwave signals with different intra-pulse modulation formats, i.e., phase-shift keying (PSK), frequency-shift keying (FSK) and linear frequency modulation (LFM).

This work intends to present another way to implementing intra-pulse measurements with the photonic IFM. The proposed approach is to measure the IF modulated by envelope of the signal. The IF signal has frequency purity because this device is considered a locally IF generator [13].

The process of intra-pulse detections of wideband RF signals occurs in three steps: translation of the signal from RF to the optical range; removing the optical carrier and upper sideband by filtering in Bragg grating; and injecting the lower optical sideband in the Mach Zehnder Interferometer (MZI). The MZI presents polarization maintenance and size difference between its arms, thus generating time difference between the signals. The signals from the two arms undergo constructive interference and couple into a low-speed photodetector.

The translation of the signal from RF to the optical range occurs in optical phase modulator. The phase modulation brings an advantage of avoiding voltage drift at the bias. This device does not need of the bias voltage and has lower optical insertion loss than the Mach-Zehnder modulator (MZM) [14]. The schematic diagram of the experimental set-up is present in Fig. 1. Another advantage for using low speed photodetector is transimpedance amplification. The circuit at output of this device is considered as a low pass filter because of the low frequency of the output signal (few hundred MHz). The consequence is possibility of using low frequency circuits with low-speed ADC. The proposed optical circuit may later evolve into a PIC due to the few components and their integrability [15].

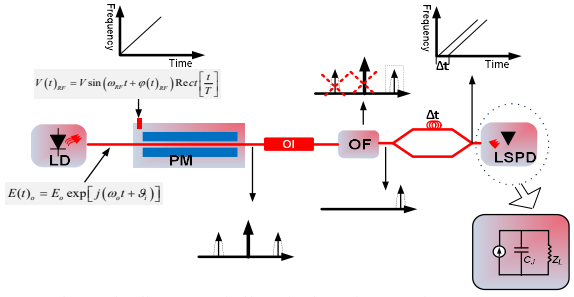

Fig. 1. Schematic diagram of all optical RF intra-pulse IFM. LD – Laser Diode, PM – Phase Modulator, OI – Optical Isolator, OF – Optical Filter, LSPD - Low Speed Photodetector, C_j – Junction Capacitance and Z_i - Load Impedance.

II. Theoretical Modeling of The Intra-pulse All Optical IFM

The optical carrier generated by a laser diode is represented by the phasor of its electric field equal to:

$$E(t)_O = E_O exp\,[j(\omega_O t + \varphi_i)], \tag{1}$$

where E_O is the electric field amplitude of the signal from the laser diode, ω_O is angular frequency and the phase is φ_i. To facilitate the analysis of the $E(t)_O$ field, the φ_i phase is considered equal to zero.

Considering an RF electrical signal with its time varying phase, injected into the RF input of a phase modulator, defined as:

$$V(t)_{RF} = V\,\mathrm{sen}(\omega_{RF} t + \varphi_{RF}(t))Rect\left[\frac{t}{T}\right], \tag{2}$$

where V is the amplitude of the incident RF signal is represented by $V(t)_{RF}$, its angular frequency is given by ω_{RF} and $\varphi_{RF}(t)$ is the time varying phase. The time limitation is given by $Rect\left[\frac{t}{T}\right]$ and its value is comprised of -T/2 < t < T/2, where the parameter T is the RF signal pulse width. In the phase modulator, the output of the optical signal is:

$$E(t)_M = E_O\,exp[j\omega_O t] \times exp\left[jm\,\mathrm{sen}(\omega_{RF} t + \varphi_{RF}(t))Rect\left[\frac{t}{T}\right]\right]. \tag{3}$$

The modulation index of the phase modulator, *m*, is given by:

$$m = \frac{V}{V_\pi}\pi, \tag{4}$$

where V_π is the drive voltage of the optical phase modulator. At (3) is applied the Jacobi-Anger expansion, it became:

$$E(t)_M = Rect\left[\frac{t}{T}\right] x \left\{\sum_{g=-\infty}^{g=\infty} E_O J_g(m)\,exp\left[j\left(\omega_O t + g(\omega_{RF} t + \varphi_{RF}(t))\right)\right]\right\} \tag{5}$$

At (5) is the Bessel functions of first kind and order g[th]. Considering special modulator operating condition known as the small signal operating mode was considered, where $m \ll 1$, the (5) has the Bessel function series truncated from values of g = { -1.0.1} [14]. Thus, the modulator output signal in the small signal operating range can be expressed by:

$$E(t)_M \cong Rect\left[\frac{t}{T}\right]\{E_O J_0(m)exp\,[j(\omega_O t)] + E_O J_1(m)exp\left[j\left(\left(\omega_{mod} t + \varphi_{RF}(t)\right)\right)\right] - E_O J_1(m)exp\left[j\left(\left(\omega_{mod} t - \varphi_{RF}(t)\right)\right)\right]\}, \tag{6}$$

where ω_{mod} is the angular frequency of the optical modulated signal. It is given by $\omega_{mod} = \omega_0 + \omega_{RF}$.

This phase modulator output signal is then coupled to the optical filter. The uniform Bragg grating was considered as the optical filter for mathematical formulation. Its behavior is postulated as a uniformly ideal step function. It is employed at the operating point of Fig. 2. The optical signal is fully reflected only in a wavelength range called stopband; this is rejected. The response of this filter is as follows $\tau(\omega)exp\,[j\varphi]$. The variable $\tau(\omega)$ represents the coefficient of grating wave transmission and $\varphi(\omega)$ the phase depending on the angular frequency of the optical signal. The tuning is effective when the angular frequency of the optical carrier, ω_0, is equal to the angular frequency of the stopband corresponding to its upper limit, ω_s.

The value of $\tau(\omega)$ is postulated equal to zero when $\omega_0 - \omega_i \leq \omega \leq \omega_s$, the ω_i is the lowest limit of the grating stopband, in other words, when it is covered by the stopband is discarded. For the other values of ω the postulated value of $\tau(\omega) \cong \tau$ and $\varphi(\omega) = \varphi$. The electrical field coupled to the photodetector is expressed as follows:

$$E(t)_T \cong \tau E_1 J_1(m) \times \left\{exp\left[j\left(\left(\omega_{mod}t + \varphi_{RF}(t)\right) + \varphi\right)\right]\right\} Rect\left[\frac{t}{T}\right]. \quad (7)$$

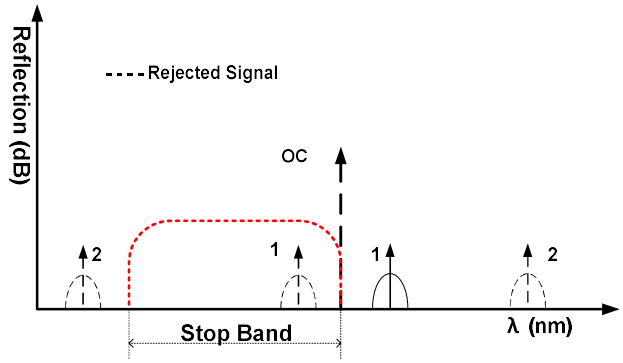

Fig.2: Schematic diagram of the behavior of a uniform, DC-apodised Bragg grating. OC – Optical Carrier.

The optical filtering of signal 1, observed in Fig. 2, allows the phase modulation to be converted to intensity only when the signal has its lower lateral band and the optical carrier covered by the Bragg grating stopband. If the signal is not in this situation (signal 2 in Fig. 2), it will not be converted to intensity modulated signal and will not be detected by the photodetector. Only signals that have had their lower sideband reflected by the grid will be photodetected. This process guarantees a selective grid for the receiver. The beating of the spectral components of the upper sideband to each other in the photodetector will ensure the lowering of the signal to the baseband. The alternating current signal in the photodetector output is because it is a video band that has a small band, which allows obtaining a smaller noise figure for the device.

The electrical field described by (7) that comes out of the uniform Bragg grating and falls on the Mach Zehnder interferometer undergoes a 50/50 balanced signal division and on one of its arms receives a time delay equal to Δt as shown in Fig. 3 and described by:

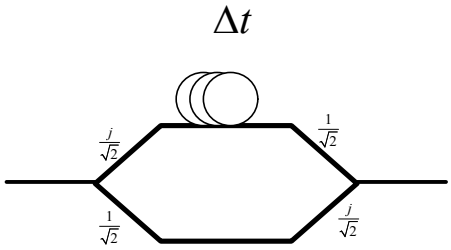

Fig.3: Schematic diagram of Mach Zehnder's mathematical interferometer modeling.

$$E(t)_{MZI} \cong \frac{\tau E_1 J_1(m) j}{2} \times \left\{exp\left[j\left(\omega_{mod}(t-\Delta t) + \varphi_{RF}(t-\Delta t)\right)\right]\right\} Rect\left[\frac{t-\Delta t}{T}\right] + \frac{\tau E_1 J_1(m) j}{2} \times \left\{exp\left[j\left(\omega_{mod}t + \varphi_{RF}(t)\right)\right]\right\} Rect\left[\frac{t}{T}\right]. \quad (8)$$

At the (8), two parcels are observed inside the bracket, the first indicates the signal that propagated in the long branch. The second parcel represents the propagated signal in the short branch. The signal described in (8) considering that the rectangular function will assume a new interval (that of the smallest interval, since the amplitude is equal) one has:

$$E(t)_{MZI} \cong \frac{\tau E_1 J_1(m)}{2} Rect\left[\frac{t-\Delta t}{T}\right] \times \left\{ \begin{array}{c} exp\left[j\left(\omega_{mod}t + \varphi_{RF}(t) + \frac{\pi}{2}\right)\right] \\ +exp\left[j\left(\omega_{mod}(t-\Delta t) + \varphi_{RF}(t-\Delta t) + \frac{\pi}{2}\right)\right] \end{array} \right\} \quad (9)$$

The optical signal intensity injected in the photodetector is defined from the relationship [16]:

$$S(t) \propto E_{MZI}(t) E_{MZI}{}^*(t), \quad (10)$$

where the asterisk sign, *, means conjugated complex of the field $E_{MZI}(t)$. Applying (9) to (10) results:

$$S(t) \propto \alpha \left(\frac{\tau E_1 J_1(m)}{2}\right)^2 Rect^2\left[\frac{t-\Delta t}{T}\right] \times \left\{ \begin{array}{c} exp\left[j\left(\omega_{mod}t + \varphi_{RF}(t) + \frac{\pi}{2}\right)\right] \\ +exp\left[j\left(\omega_{mod}t - \omega_{mod}\Delta t + \varphi_{RF}(t-\Delta t) + \frac{\pi}{2}\right)\right] \end{array} \right\} \times \left\{ \begin{array}{c} exp\left[-j\left(\omega_{mod}t + \varphi_{RF}(t) + \frac{\pi}{2}\right)\right] \\ +exp\left[-j\left(\omega_{mod}t - \omega_{mod}\Delta t + \varphi_{RF}(t-\Delta t) + \frac{\pi}{2}\right)\right] \end{array} \right\} \quad (11)$$

The accumulated optical losses are represented by α. Developing (11) and making the common terms in evidence, it is obtained:

$$S(t) \propto \alpha\left(\frac{\tau E_1 J_1(m)}{2}\right)^2 Rect^2\left[\frac{t-\Delta t}{T}\right] \left\{2+exp\left[j\left(\omega_{mod}\Delta t+\left(\varphi_{RF}(t)-\varphi_{RF}(t-\Delta t)\right)\right)\right] +exp\left[-j\left(\omega_{mod}\Delta t+\left(\varphi_{RF}(t)-\varphi_{RF}(t-\Delta t)\right)\right)\right]\right\}. \quad (12)$$

The current output of the photodetector is:

$$i(t)=\frac{\alpha}{2}P_0\Re\left(\tau J_1(m)\right)^2 Rect^2\left[\frac{t-\Delta t}{T}\right] \left\{1+cos\left(\omega_{mod}\Delta t+\left(\varphi_{RF}(t)-\varphi_{RF}(t-\Delta t)\right)\right)\right\}, \quad (13)$$

where the $\Re$ is the photodetector responsivity and the P_0 is the optical power at the laser diode output given by relation $P_0 \propto E_0^2$. The Rect. function amplitude value was postulated to be the unity and (13) became:

$$i(t)=\frac{\alpha}{2}P_0\Re\left(\tau J_1(m)\right)^2 Rect\left[\frac{t-\Delta t}{T}\right] x\left\{1+cos\left(\omega_{mod}\Delta t+\left(\varphi_{RF}(t)-\varphi_{RF}(t-\Delta t)\right)\right)\right\}. \quad (14)$$

The current at output of the device for the LFM signal is:

$$(t)=\frac{\alpha}{2}P_0\Re\left(\tau J_1(m)\right)^2 Rect\left[\frac{t-\Delta t}{T}\right] x\left\{1+cos\left(\omega_{mod}\Delta t+\mu(t^2-t^2+2t\Delta t-\Delta t^2)\right)\right\}. \quad (15)$$

where the RF phase is given by $\varphi_{RF}(t)=\mu t^2$ and μ is the RF frequency variation rate. The parcel corresponding to the AC signal is:

$$i(t)=\frac{P_0}{2}\Re\alpha\tau^2 J_1^2(m)Rect\left[\frac{t-\Delta t}{T}\right] x\ cos\left((\Delta t\omega_{mod}-\mu\Delta t^2)+Wt\right), \quad (16)$$

where $W=2\mu\Delta t$. Development (16):

$$i(t)=\frac{P_0}{2}\Re\alpha\tau^2 J_1^2(m)Rect\left[\frac{t-\Delta t}{T}\right] x\ cos\left((\Delta t\omega_{mod}-\mu\Delta t^2)\right)cos(Wt) -sin\left((\Delta t\omega_{mod}-\mu\Delta t^2)\right)sin(Wt), \quad (17)$$

and if this term $\Delta t\omega_{mod}-\mu\Delta t^2$ becomes multiple of $2\pi k$, where k is an integer number, the AC parcel is:

$$i(t)=\frac{P_0}{2}\Re\alpha\tau^2 J_1^2(m)Rect\left[\frac{t-\Delta t}{T}\right]cos(Wt). \quad (18)$$

The AC current at (18) describes a signal that has the IF modulated by a Rect. function with time duration *T-Δt*. The time variation, *Δt*, is known, then it is possible to measure the PW, IRP, PA and μ. The W parameter can vary by the time when the RF signal is nonlinear modulated. The frequency pattern can be predicted and if it happens, it will be known. For all these cases can be measured when the output of the device is coupled to the simple ADC, because the IF output is low frequency (MHz or kHz, it depends on the frequency modulation). The value of the *Δt* must be much lower than *T* value and higher than transition time of the signal (when the signal has discrete variation, like a PSK modulation). The pattern observed at PSK modulation signal is the time variation of amplitude induced by the time phase variation at (14). The pattern perceived by ASK modulated signal will be, only, its envelope (Rect. function), because the time phase variation at (14) is zero. The (18) becomes:

$$i(t)=\frac{P_0}{2}\Re\alpha\tau^2 J_1^2(m)Rect\left[\frac{t-\Delta t}{T}\right]. \quad (19)$$

III. Experiment and Analysis of Results

An optical circuit was assembled based on the approach presented in Section II and implemented, as shown in Fig. 4, with the objective of demonstrating the concept of photonic intra-pulse IFM for RF signals. This optical circuit was assembled with commercially available components. The optical source used was the DFB laser that operated at around 1551.5 nm. The optical signal from the laser diode is coupled into a 20 GHz PM. A radar pulse generator with an operating range of 0.5 to 18 GHz sends signals to the PM input to modulate the optical signal from the DFB laser. The modulated optical signal leaving the PM enters port 1 of the 3-port optical circulator. This signal leaves the circulator at port 2 and is coupled into a uniform Bragg grating that operates at around 1551.5 nm, with a rejection band of 50 GHz, as shown in Fig. 4 and 5. In the Bragg grating, the phase-modulated optical signal undergoes optical filtering of the carrier and the lower sideband, where they are reflected and exit through port 3 of the optical circulator, to be discarded. The upper sideband is transmitted from the FBG output to the unbalanced IMZ. The signal at the output of the unbalanced IMZ is composed of the sum of the upper sideband and its delayed version, to then be incident on a low-speed photodetector. The uniform Bragg grating used has a slew rate of 2 dB/GHz, as shown in Fig. 5. The MF employed has a V_π value equal to 10.5 V at a frequency of 17 GHz. The optical carrier was adjusted to operate with 100 mW of power, and the measured optical losses were 13 dB. The laser linewidth is 1 MHz. Aiming to guarantee the small signals condition, RF signals were adjusted to 0 dBm power at the MF input. The unbalanced IMZ delay was obtained by using 200 m of optical fiber conditioned on a reel, which provides a delay of 1 μs.

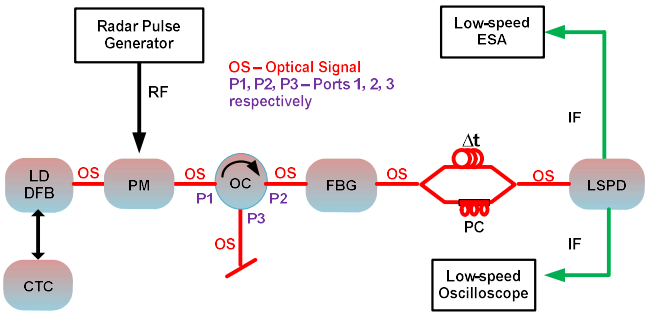

Fig. 4. Schematic diagram of the photonic IFM demonstration setup. LD - Laser diode, DFB - Distributed Feedback, CTC - Temperature and current controller, FBG - Fiber Bragg grating, OC - Optical circulator, LSPD – Low-speed photodetector, PC – Polarization controller, and ESA – Electric Spectrum analyzer.

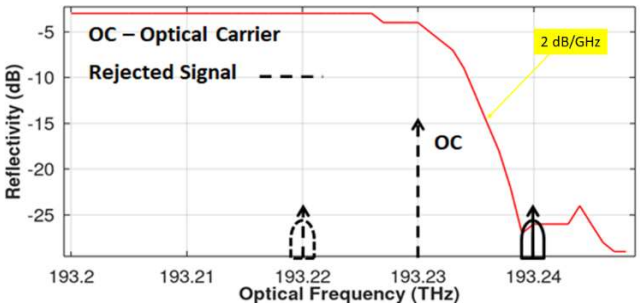

Fig. 5. Right side of rejection passband optical filter, cut right on the center frequency. This center is around 193.2 THz and 1551.7 nm.

The test of the conceptual intra-pulse IFM was performed by generating one signal with a chirp rate of 30 MHz/µs and PW of 10 µs. Applying the expression to calculate the IF based on the expression W =µΔt, the expected value for the IF is obtained, which in this case is 30 MHz. The spectrum measured for this signal is shown in Fig. 6. It should be noted that the 3 dB criterion of the RF signal power at the system output was used to measure the IF.

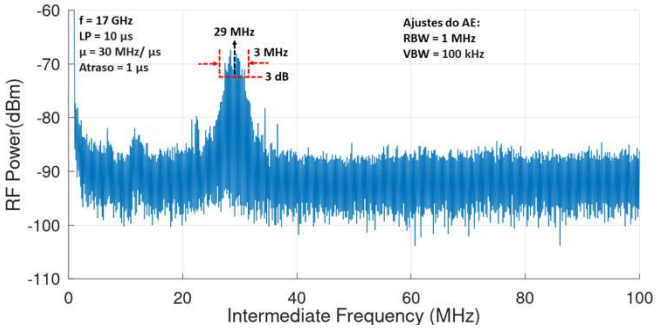

Fig. 6 - Measurement obtained with the low frequency spectrum analyzer. The measured IF value was 29 MHz with an uncertainty of 3 MHz. BW – EA bandwidth; RBW – EA bandwidth resolution; and VBW – EA video bandwidth.

The result observed in Fig. 6 allows us to prove the concept of measuring linear frequency variation by means of an IF. The value of this IF is based on the value of the chirp rate and the delay between arms of the unbalanced IMZ. This IF value was measured at 29 MHz centered in an uncertainty region of 3 MHz.

IV CONCLUSIONS

This article presented a MWP approach to RF measure chirp rate of RF intra-pulsed modulated. This proposal indicates that it is possible, according to mathematical development, to measure pulse width and pulse repetition interval in time domain. In mathematical formulation we can perceive a rectangular function. The next challenge is to measure in time domain pulse width, pulse repetition interval, and sensitivity. This optical circuitry uses a phase modulator; it brings the advantage do not need to employ a bias voltage control circuit compared with the ones that use intensity modulators. The proposed optical circuit brings the benefit of employing simpler digitizers, reducing system latency, and has the possibility of being transformed into a photonic integrated circuit.

REFERENCES

[1] J. Capmany and D. Novak, “Microwave photonics combines two worlds,” *Nature Photonics*. 2007, doi: 10.1038/nphoton.2007.89.

[2] D. L. Adamy, *Introduction to electronic warfare modeling and simulation*. Institution of Engineering and Technology, 2006.

[3] B. Lu *et al.*, “Photonic-assisted intrapulse parameters measurement of complex microwave signals,” *J. Light. Technol.*, 2018, doi: 10.1109/JLT.2018.2839354.

[4] P. Minzioni *et al.*, “Roadmap on all-optical processing,” *J. Opt. (United Kingdom)*, 2019, doi: 10.1088/2040-8986/ab0e66.

[5] G. L. Fudge, M. A. Chivers, S. Ravindran, R. E. Bland, and P. E. Pace, “A reconfigurable direct RF receiver architecture,” 2008, doi: 10.1109/ISCAS.2008.4541994.

[6] T. Chalvatzis, E. Gagnon, and J. S. Wight, “On the effect of clock jitter in if and RF direct sampling systems,” 2005, doi: 10.1109/NEWCAS.2005.1496679.

[7] G. L. Fudge, R. E. Bland, M. A. Chivers, S. Ravindran, J. Haupt, and P. E. Pace, “A Nyquist folding analog-to-information receiver,” 2008, doi: 10.1109/ACSSC.2008.5074464.

[8] J. Meng, M. Miscuglio, J. K. George, A. Babakhani, and V. J. Sorger, “Electronic bottleneck suppression in next-generation networks with integrated photonic digital-to-analog converters,” *Adv. Photonics Res.*, vol. 2, no. 2, p. 2000033, Feb. 2021, doi: 10.1002/adpr.202000033.

[9] X. Liu and Y. Zhao, “Wideband radar frequency measurement receiver based on FPGA without mixer,” *IEICE Trans. Inf. Syst.*, 2019, doi: 10.1587/transinf.2018EDL8161.

[10] R. Maram, S. Kaushal, J. Azaña, and L. R. Chen, “Recent trends and advances of silicon-based integrated microwave photonics,” *Photonics*. 2019, doi: 10.3390/photonics6010013.

[11] M. A. Zobair, B. Boroomandisorkhabi, and M. Esmaeelpour, “Recent Advances in Multitone Microwave Frequency Measurement,” *Sensors*, vol. 25, no. 12, p. 3611, Jun. 2025, doi: 10.3390/s25123611.

[12] L. A. Bui, “Recent advances in microwave photonics instantaneous frequency measurements,” *Prog. Quantum Electron.*, 2020, doi: 10.1016/j.pquantelec.2019.100237.

[13] G. Qi *et al.*, “Phase-noise analysis of optically generated millimeter-wave signals with external optical modulation techniques,” *J. Light. Technol.*, 2006, doi: 10.1109/JLT.2006.884990.

[14] A. Yariv and P. Yeh, *Photonics: optical electronics in modern communications*, 6th ed. Oxford University Press, 2006.

[15] Y. Tao *et al.*, “Fully On-Chip Microwave Photonic Instantaneous Frequency Measurement System,” *Laser Photon. Rev.*, vol. 16, no. 11, p. 2200158, Nov. 2022, doi: 10.1002/lpor.202200158.

[16] D. M. Pozar, *Microwave engineering*, 4th ed. 2012.